agronomy

MDPI

Article

Is the Subsurface Drip the Most Sustainable Irrigation System for Almond Orchards in Water-Scarce Areas?

Francisco Montoya [1,2,*], Juan M. Sánchez [3], José González-Piqueras [3] and Ramón López-Urrea [1]

[1] Instituto Técnico Agronómico Provincial (ITAP) and FUNDESCAM, Parque Empresarial Campollano, 2ª Avda. Nº 61, 02007 Albacete, Spain; rlu.itap@dipualba.es
[2] Regional Center of Water Research (CREA), University of Castilla-La Mancha, Av. España, s/n, 02071 Albacete, Spain
[3] Department of Applied Physics, Regional Development Institute (IDR), University of Castilla-La Mancha, Av. España, s/n, 02071 Albacete, Spain; juanmanuel.sanchez@uclm.es (J.M.S.); jose.gonzalez@uclm.es (J.G.-P.)
* Correspondence: fms.itap@dipualba.es

Abstract: The expansion of irrigated almond orchards in arid and semi-arid areas with scarce water available raises key issues related to the sustainability of the water resources. A 3-year field experiment was conducted on a commercial young almond orchard located in the southeast of Spain to study the effect of two drip irrigation systems (surface, DI and subsurface, SDI) on almond crop growth and their physiological responses under fully-irrigated conditions. Crop evapotranspiration (ET_c) and its components (crop transpiration, T_c and soil evaporation, E_s) were monitored as well as the irrigation water and nitrogen productivities. To estimate ET_c, a simplified two-source energy balance (STSEB) approach was used. Although a lower irrigation water amount was applied in SDI compared to DI (differences between 10% and 13.8%), the almond crop growth and physiological responses as well as the yield components and kernel yield showed no significant differences. The ET_c estimates resulted in small differences for spring and fall periods (0.1–0.2 mm day^{-1}) for both treatments, while differences were significant during higher ET_o periods (May–August), being 1.0–1.3 mm day^{-1} higher for the DI treatment than for the SDI treatment. The irrigation water productivity (IWP) was significantly higher in the SDI treatment than in the DI treatment. However, no significant differences between the two treatments were observed for nitrogen productivity. It can be concluded that the SDI system is a suitable strategy for irrigating almond crops, reducing consumptive water use and increasing IWP.

Keywords: plant-water status; crop evapotranspiration; simplified two-source energy balance; irrigation water productivity; nitrogen productivity

Citation: Montoya, F.; Sánchez, J.M.; González-Piqueras, J.; López-Urrea, R. Is the Subsurface Drip the Most Sustainable Irrigation System for Almond Orchards in Water-Scarce Areas? *Agronomy* **2022**, *12*, 1778. https://doi.org/10.3390/agronomy12081778

Academic Editor: Maria do Rosário Cameira

Received: 23 June 2022
Accepted: 26 July 2022
Published: 28 July 2022

1. Introduction

The sustainable development goals defined by the United Nations in 2015 focus, through several aspects, on significantly increasing the water use efficiency in all sectors by 2030, ensuring the sustainability of withdrawals and freshwater supply in water-scarce areas [1]. This is directly related to irrigated agriculture, as it is the primary water-consuming sector, accounting for about 70% of the total. In addition, the expansion of crops with high water requirements such as almond trees, which have undergone a significant increase in almond growing area over the last decade (between 35 and 56% [2]), may be limited in areas with scarce water resources, and it is thus mandatory to establish practices that improve water use efficiency. Moreover, climate change predictions for the Mediterranean basin forecast an increase in evaporative demand and increasingly erratic and extreme rainfall events, driving an eventual reduction in water availability [3]. Therefore, technicians and researchers in agricultural irrigation are encouraged to develop technologies and management tools for more sustainable water use, thus saving water and improving the water use efficiency whenever possible.

Several reports and research papers have conducted in-depth studies and reviews on improving the water productivity and water use efficiency using different methods, technologies, and strategies to minimize non-consumptive water use (runoff and deep percolation) as well as non-beneficial water consumption (soil evaporation, E_s (Appendix A) or weed consumption) by crops [4–6]. In this sense, transferring operative tools and practices that make orchard irrigation management easier and more accurate for almond growers and technicians is a key issue in optimizing the irrigation water resources. Thus, a proper separation between E_s and crop transpiration (T_c, Appendix A) is required in these kinds of discontinuous canopies [7] to generate net water savings. In addition, deficit irrigation may be a useful technique in almond crop, as this has shown an excellent adaptability to different situations of water availability [8–10]. Nevertheless, many works carried out in almond orchards have demonstrated that irrigation can be considered the main limiting factor in terms of yield and nut quality [11].

Strategies to reduce soil evaporation are also a challenge for addressing and mitigating water scarcity, and consequently, for improving crop-water use efficiency. Some practices focused on minimizing E_s include proper crop management (such as increasing plant density and canopy size) using soil mulching (both organic and plastic materials) and suitable soil management (no-till), or by applying irrigation water from the subsurface drip irrigation system [4]. Thus, the main methodologies to address this challenge range from a simple soil water balance (SWB, Appendix A), typically using the "two step" approach [12,13], to surface energy balance (SEB, Appendix A) approaches using both ground (such as Eddy-covariance, EC, and Bowen ratio, BR, systems) and remote sensing techniques (based on either optical or thermal multispectral imagery; [14–18]). With respect to the SEB approaches, two-source energy balance (TSEB) models, together with ground measurements of soil and canopy temperatures, biophysical information, and meteorological data, have provided good results in field crops [19–23], vineyards [17,24–27] and almond crop [28]. Using a simplified version of the two-source approach (STSEB, Appendix A), Sánchez et al. [17] reported that E_s reached 35–40% of the total crop evapotranspiration (ET_c, Appendix A) in a mature vineyard, while in a young almond orchard under a drip irrigation system, Sánchez et al. [28] found that this ratio fell to 26% of the total ET_c using the same technique.

The two last decades have witnessed renewed interest in using the subsurface drip irrigation (SDI, Appendix A) system for irrigated agricultural systems, since it is an operative tool that allows, among other advantages, to directly and efficiently apply water and nutrients within the crop root zone [29]. Thus, SDI, versus surface drip irrigation (DI, Appendix A), allows consumptive irrigation water use to be optimized, since the irrigation-water evaporation and runoff losses are minimized if this system is properly designed, installed, and managed [30,31]. In a recent review on the adoption of SDI systems in the USA, Lamm et al. [29] reported that, in general, SDI allowed the net crop water requirements to be met, with water savings between 15–60% compared to other irrigation systems (DI, sprinkler, and furrow irrigation), where crop yield levels (either field and horticultural crops) were maintained or improved in several studies. Therefore, water productivity in terms of the use of irrigation water (IWP, Appendix A) as well as the use of fertilizers was significantly increased [29]. In the case of fruit trees and vineyards, very few studies have compared SDI and DI. Ayars et al. [32] found that pomegranate yield and IWP were increased and there was less weed pressure for SDI vs. DI. Ma et al. [33] showed that Direct Root Zone irrigation (DRZ, Appendix A), which is a modification of SDI, increased wine grape yield and WP by 9–12%, compared to DI. Meanwhile, Romero et al. [34] combined the use of SDI and certain regulated deficit irrigation (RDI, Appendix A) techniques in a mature almond orchard. These authors obtained higher water application efficiency with SDI, although RDI caused significant reductions in kernel yield compared to the reference treatment.

Given this context, the aim of the present study was to analyze whether it is possible to save water without yield losses in young almond trees by using subsurface drip

irrigation compared to the traditional surface drip irrigation system, in order to improve the sustainability of irrigated almond orchards in water-scarce areas. For this purpose, the following objectives were established under no soil water limitations: (a) to study almond crop growth and physiological responses to SDI and DI systems; (b) to quantify and compare the ET_c and its components between irrigation systems using two-source energy balance modeling; and (c) to analyze the effects of both irrigation systems on the irrigation water and nitrogen productivity (IWP and NP, respectively, Appendix A) and crop-water use efficiency (WUE_c, Appendix A).

2. Materials and Methods

2.1. Site Description

A field experiment was carried out over three growing seasons (2019–2021) in a commercial 12.5-ha young almond orchard located in the southeast of Albacete province, Spain (38°29′3″ N, 1°47′9″ W, 550 m a.s.l.; Figure 1). The soil, classified as Aridisol [35], is of a fine-loam texture to a depth of 1.2 m and with a petrocalcic horizon below this. It has low organic matter (~1%) and grave content (<2%), is slightly saline (~0.40 dS m^{-1}), and has a high total carbonate content (36–38%) and nitrate concentration of 1.84 ppm. The soil hydraulic characteristics were estimated using the soil water characteristics program (v. 6.02.74; [36]), where the soil analysis data belonging to two differentiated soil horizons were used (till and no-till depths; Table 1). The irrigation water used during the experimental period was classified as good quality for irrigation (Scott's index), with an average electrical conductivity of 1.10 dS m^{-1} and a nitrogen concentration of around 13 ppm.

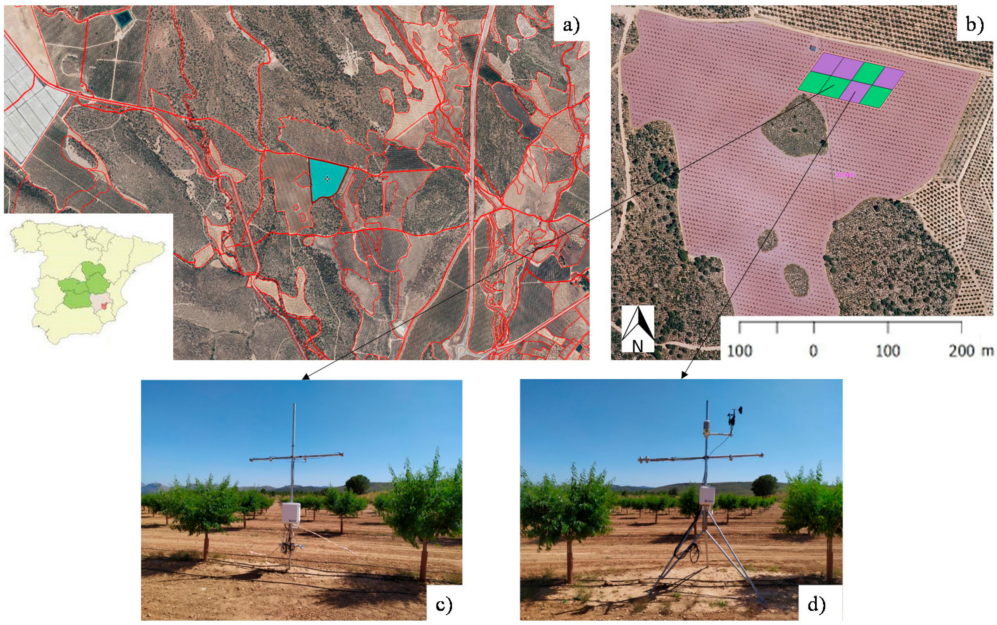

Figure 1. (**a**) The location of the commercial almond orchard; (**b**) experimental layout on the almond orchard (green squares: surface drip irrigation system, DI; purple squares: subsurface drip irrigation system, SDI); (**c**) fixed mast with a set of thermal InfraRed thermometers in an elementary plot of the DI treatment; (**d**) fixed mast with a set of thermal InfraRed thermometers and meteorological sensors in an elementary plot of the SDI treatment.

Table 1. The hydraulic characteristics of the soil experimental plot.

Soil Depth (m)	FC (%)	PWP (%)	Saturation (%)	Sat. Hydr. Conduct. (mm h^{-1})	Bulk Density (t m^{-3})
0.00–0.30	24.6	12.9	42.8	13.9	1.52
0.30–1.20	26.3	14.1	43.7	15.9	1.49

FC—field capacity; PWP—permanent wilting point; Sat. Hydr. Conduct.—saturated hydraulic conductivity.

The study area has a Mediterranean semi-arid climate with a low annual rainfall (319.6 mm), mainly concentrated in spring and fall; and a large yearly cumulative grass reference evapotranspiration (ET_o, Appendix A, of around 1259 mm), calculated using the FAO56 Penman-Monteith (FAO56-PM) equation [12]. Previous studies in the experimental site based on lysimeter observations reported this method performed well [37]. Meteorological data during the 3-year experiment were continuously measured on site, starting April 2019. All instruments were set up at a height between 2.5 and 4.0 m above the ground surface, and weather data were registered at 15 min, hourly, and daily time steps. The variables measured were as follows: incoming and surface-reflected short-wave radiation (model CM14, Kipp & Zonen, Delft, The Netherlands), incoming and outgoing long-wave radiation (model CG2, Kipp & Zonen, Delft, The Netherlands), air temperature/relative humidity (HC2A-S3, Campbell Scientific Instrument, Logan, UT, USA), wind speed and direction (03002 Wind Sentry, R.M. Young, Traverse City, MI, USA), and rainfall (52203 Rain Gauge, R.M. Young, Traverse City, MI, USA). All meteorological data were recorded with a CR1000 datalogger (Campbell Scientific Instrument, Logan, UT, USA). In addition, ET_o data were recorded during the three seasons from the "Ontur" meteorological station, which is the nearest station belonging to the Spanish network of the agroclimatic information system for irrigation [38].

2.2. Orchard Description and Management

The study was conducted in young almond trees (*Prunus dulcis* (Mill.) D.A. Webb) planted in March 2018 with cv. 'Penta' grafted onto the GF-677 rootstock. The tree spacing was 6.0 m (inter-row) and 5.0 m (within row), resulting in a tree density of 333 plants ha^{-1}. A vase-training system was used to configure the canopy architecture where several green-pruning tasks were carried out across the three seasons to encourage fruiting.

Using fertigation, the almond orchard was fertilized at a rate of 56-16-30 kg ha^{-1} of N-P-K, 56-32-68 kg ha^{-1} of N-P-K and 132-75-116 kg ha^{-1} of N-P-K in each experimental season (2019, 2020, and 2021, respectively). The first 0.10 m of the soil depth was tilled to control the weeds, and pest and disease effects were managed according to cultural practices typically implemented in the region to establish potential crop performance. In the first year of the study, there was no production as the trees were only 1 year old. In the second and third experimental seasons, the almond crop was harvested once 100% of the fruits had shown hull split and were partially dried (i.e., 1 September 2020 and 27 August 2021).

Two treatments were designed to supply 100% of the irrigation-water requirements throughout the almond growing season using two drip-irrigation systems. The treatments assessed were DI (surface drip irrigation system) and SDI (subsurface drip irrigation system). The experimental design was a complete block randomized layout of the two treatments already set up with four replicates (eight elementary plots; Figure 1b). Each elementary plot consisted of five rows with six trees each resulting in 900 m^2 (total of 30 almond-trees).

The almond orchard was irrigated from two parallel drip lines per tree row, each one separated 0.80 m from the almond-tree. The flow of the self-compensating emitters was 4.0 L h^{-1} (AmnonDrip PC, CNL & PC AS, NaanDanJain Company, Naan, Israel). These were placed 0.75 m apart, and, thus, both systems were designed to apply 1.78 mm h^{-1}. The buried drip lines (SDI) were installed to 0.35 m depth by the farmer. A flow meter

at the head of each treatment allowed for the irrigation water depth applied during the irrigation season to be controlled.

2.3. Almond Tree Development, Physiological Measurements, and Soil Water Content Evolution

Two trees located in the central row of each elementary plot were used for monitoring the crop growth, physiological and development variables, and soil water content evolution. However, six trees of each elementary plot were sampled at harvest time.

The aboveground almond tree variables measured in each elementary plot during the study period were: (a) the almond phenological stage, following the scale designed by Thomas [39]; (b) the canopy architecture evolution, measuring the horizontal diameters of the canopy and tree height with a measuring tape; (c) the fraction of ground covered by the canopy (f_c, Appendix A); and (d) measurements of the plant water status.

The main phenological stages identified were: (I) from swollen bud to fruit set; (II) from fruit set to early pit hardening; (III) from early pit hardening to hull split (harvest); and (IV) from harvest to 50% of leaves fall. During the three experimental years, phenology data were collected every 10–15 days starting by late-February until mid-December.

To determine f_c over the study period, two methodologies were used. During the first season, a 12-Mp digital camera, mounted on a hand-held aluminum pole, was used to capture nadir views 3.0 m above the ground surface. Two trees per elementary plot, together with a white reference of known surface area, were photographed. Using the CANOPEO software [40], a green canopy cover was computed (Figure 2a), and the reference surface area was used to extrapolate this value to the planting frame (30 m^2 per plant). In 2019, eight sampling days were implemented, which coincided with the sampling of both horizontal diameters and the height of the tree.

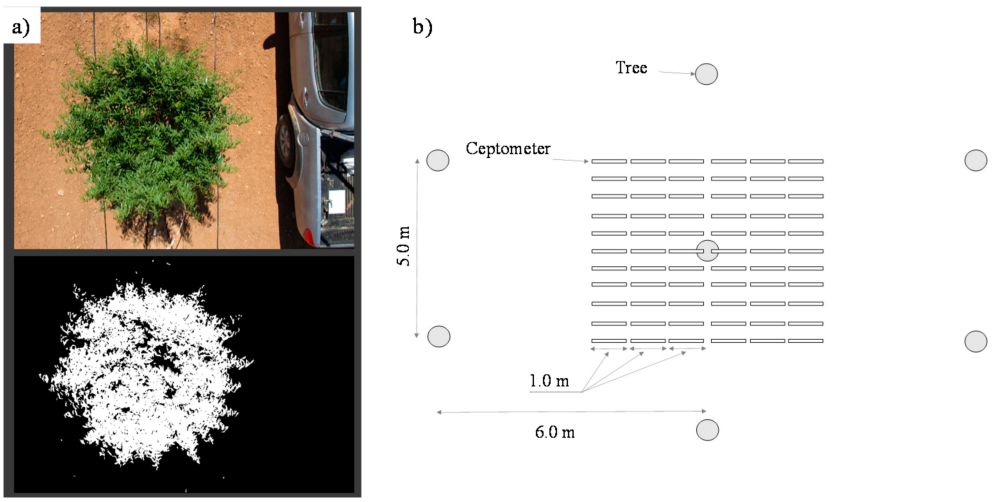

Figure 2. (**a**) An example for the classification of the fraction of ground covered by the canopy using CANOPEO software; (**b**) A schematic representation of the almond tree spacing and positions where PAR measurements were taken by SunScan^{TM}.

Another indicator used to evaluate the f_c was the fraction of intercepted photosynthetic active radiation (f_{IPAR}, Appendix A), which was measured during the two last growing seasons. The photosynthetically active radiation (PAR, Appendix A) data were collected in one central tree in each experimental plot close to midday. Measurements were taken using a SunScan^{TM} canopy analysis system (Delta-T Devices Ltd., Cambridge, UK). F_{IPAR} was calculated as an average ratio from the PAR data below and above the tree canopy, following a methodology similar to that described by Auzmendi et al. [41]. Thus, a fixed mesh of 66 reading points, which covered the planting frame of a tree, was established (Figure 2b). For below-canopy data, readings were taken by placing the ceptometer (probe length 1.0 m) in a horizontal position at ground level, and perpendicularly to the row (Figure 2b). The above-canopy readings were also 66, which were taken with the sunlight

sensor. In both experimental years, the trees were sampled and data collected eight times, also coinciding with the sampling of the canopy architecture. The f_{IPAR} measurements were converted to f_c considering the mean angle of the sun above the horizon during the measuring period (i.e., date of year and mean hour of readings in each sampled tree) [42,43].

The tree water status was determined from the midday steam water potential (Ψ_s, Appendix A). A Scholander pressure chamber (PMS Instruments; Corvallis, OR, USA), calibrated at the onset of each measuring season, was used for Ψ_s determination. Following the general recommendations of Fulton et al. [44], two shaded leaves from each elementary plot (one per tree) and close to the trunk base, were sampled. One hour before measuring, the leaves were covered with aluminum foil. This was undertaken 10, 12, and 9 times in 2019, 2020, and 2021, respectively, with most of the measurements coinciding with the former variables.

A set of four FDR sensors (10HS, Decagon Devices, Pullman, WA, USA) were installed in two elementary plots per treatment, and close to the drip line, with intervals of 0.15 m in depth, up to 0.60 m, to monitor the volumetric soil water content at depth, which was largely influenced by the irrigation events. These data were used to learn the humectation and desiccation behavior pattern where the highest density of rooting-soil is usually located [34]. The FDR sensors monitored the soil moisture from the onset of the almond growth season (March 2019) up to fall 2021. The mean hourly data were recorded in a datalogger (EM50, Decagon Devices, Pullman, WA, USA).

2.4. Kernel Yield Determinations and Almond Crop Productivities

During the first year of the study, only tree development was monitored, as the almond trees were 1 year old, and thus still unproductive. In the last two experimental years, almond harvest took place at the hull split stage and the start of drying (i.e., between the end of August and start of September). The six central trees in every elementary plot were harvested with an inverter-umbrella type fruit-collecting machine. The total in-shell fruit fresh weight was measured and divided by the six trees to obtain the total weight per tree (F_u, Appendix A). In addition, a randomized sample of around 2.0 kg was taken in the field to identify both the water content of the fresh fruit (H_{Ff}, Appendix A) and the kernel fraction (ratio kernel fresh weight vs. in-shell fruit fresh weight, R_k, Appendix A). A subsample of 1.0 kg was oven-dried at 65 °C until constant to determine the water content, allowing for a comparison against the standard commercial kernel yield (7% of water content; H_{Ff}). R_k was computed from a subsample of 0.3 kg, where the kernel unit weight (W_k, Appendix A; g) was measured. Thus, the former yield components were affected by the tree density (Td, Appendix A) when calculating the commercial kernel yield (Y_k, Appendix A; kg ha^{-1}), which was calculated as:

$$Y_k = F_u \times H_{Ff} \times R_k \times Td \quad (1)$$

The irrigation water productivity (IWP; kg m^{-3}), crop water use efficiency in terms of crop evapotranspiration (WUE_c; mm mm^{-1}), and nitrogen productivity (NP; kg kg^{-1} N) were calculated for both treatments. IWP was computed as the ratio between the standard commercial kernel yield and the irrigation water supplied to each crop season. However, the WUE_c was computed as the ratio between the crop evapotranspiration (ET_c) estimated from the STSEB model for the available period in each experimental year and treatment, and the total water received by the crop (i.e., irrigation + precipitation) [45]. Additionally, NP was also calculated for each treatment as the ratio between the commercial kernel yield and the units of nitrogen available for the crop (soil and water NO_{3-} N + fertilizer N) [46].

2.5. Irrigation Management

A daily irrigation schedule was computed according to the FAO56 methodology, where a simplified water balance for the root zone of the crop [12,13] was used to compute the soil water depletion ($D_{r,i}$, Appendix A). The irrigation depth (I, Appendix A) was calculated considering the soil hydraulic properties (Table 1) of the root zone (up to 1.2 m) in order to

maintain the soil water depletion between the field capacity and readily available water (RAW, Appendix A; [12]), allowing 100% of the almond crop water requirements to be met. Following the runoff curve number approach [47], the effective precipitation (P_e, Appendix A) was calculated from the daily precipitation. Deep percolation was calculated as the difference between the inputs (P_e + I) and outputs (ET_c + $D_{r,i-1}$) in the root zone. Capillary rise was not considered in the water balance because the groundwater table was much deeper than the root zone.

ET_c was computed by adding the soil evaporation and the crop transpiration (both performed by a soil water balance to the top soil layer, Z_e = 0.10 m, and to the effective depth of the root zone layer, Z_r = 1.20 m, respectively). Since the surface drip irrigation system only partially wetted the soil, and the main root density is usually located in a depth closed to the wetted bulb formed by the drip line (between 0.00 and 0.40 m depth for DI, and between 0.40 and 0.80 m depth for SDI; [34]), the first two extensions proposed by Allen et al. [48] were adopted to increase the accuracy of the total evaporation and drying process.

The average fraction of the soil wetted by surface drip irrigation was 0.12 (considering a width wetting bulb for every drip line of 0.40 m) and 0.01 for subsurface drip irrigation, while the fraction of the soil surface wetted by precipitation was 1.00. The readily evaporable water (REW, Appendix A) and the total evaporable water (TEW, Appendix A) were 8.0 and 18.1 mm, respectively. In addition, the amount of transpiration extracted from the surface layer was also considered in the soil water balance, following the methodology proposed by Allen et al. [48]. The standard basal crop coefficient (K_{cb}, Appendix A) values used were: $K_{cb\ ini}$: 0.15 during the initial crop stage (stage I); $K_{cb\ mid}$: 0.85 during the mid-season stage (stage III); $K_{cb\ end}$: 0.35 for 50% of leaves fall. Finally, a density coefficient (K_d, Appendix A) was taken into account in the daily ET_c calculation, affecting the crop transpiration. K_d was computed using the equations described by Fereres et al. [49] for fruit orchards, where the shaded area was obtained from the f_c evolution of the almond trees over the three experimental years.

2.6. Ground Radiometric Thermal Measurements. STSEB Model

Two-source energy balance modeling of crop evapotranspiration (ET_c), its soil evaporation (E_s) and canopy transpiration (T_c) contributions was conceived of as a conversion from the total latent heat flux, LE, and its soil and canopy components LE_s and LE_c, respectively, divided by the latent heat of the vaporization of water, λ (Appendix A; J kg^{-1}). The latent heat flux is a turbulent flux that can be estimated as a residual from the surface energy balance equation once the net radiation (R_n, Appendix A) and soil (G, Appendix A) and sensible heat (H, Appendix A) fluxes are calculated. For details on the equation framework and all of the required inputs and parameters, the reader is referred to Sánchez et al. [28]. In this work, ground measurements of canopy height and fractional cover, described in Section 2.3, were used to model these inputs into the STSEB framework, through a third-order polynomial adjustment.

Two sets of 3–4 thermal InfraRed thermometers (IRT, Appendix A) each (SI-121 and SI-421, Apogee Instruments, Inc., Logan, UT, USA) were deployed in two masts for the continuous thermal monitoring of the almond tree canopy and soil, covering both the DI and SDI irrigation treatments (Figure 1c,d). Three of the IRTs were assembled pointing downward with an angle of 45°, two of them to the canopy top at both the east and west side trees, and a third to the inter-row soil. The mast deployed in the DI treatment was provided with an additional IRT pointing to the exposed fraction of the soil wetted by surface drip irrigation for an accurate characterization of the soil temperature in this treatment. The full set of thermal measurements was completed with an additional IRT pointing upward to measure the downwelling sky radiance required for the atmospheric correction of all the soil and canopy temperatures. The experimental setup (location and assembling height) was designed to guarantee a representative monitoring of each target, accounting for the 18° field of view of the IRTs. Continuous 15-min IRT measurements were

collected to capture the surface energy fluxes, and then improved the daily and cumulative estimates of ET_c.

All of the measurements were corrected for atmospheric and emissivity effects following the methodology described in Sánchez et al. [50]. The emissivity values of the soil and tree canopy were measured through the temperature-emissivity separation method (TES) using a CIMEL CE-312-2 multispectral thermal radiometer (Cimel Electronique, Paris, France).

2.7. Statistical Analysis

An analysis of variance (ANOVA, Appendix A) was used to evaluate the effect of treatments on the commercial kernel yield and yield components, irrigation water productivity, and nitrogen productivity, taking into account the irrigation system treatment. The significance levels used were: $p \geq 0.05$ not significant; $0.01 \leq p < 0.05$ significant, and $p < 0.01$ very significant. The Duncan test was used to estimate whether the differences between the mean treatments were significant. Finally, the polynomial adjustment curves referring to f_c and tree height evolution as well as the statistical analysis previously described were carried out with R software [51].

3. Results

3.1. Meteorological Conditions

Compared with the long-term mean climate data in the area, most of the meteorological data from the three experimental years were similar to those typically recorded for all of the variables shown in Table 2. However, the rainfall was especially heavy during the three growing seasons, being around 28, 68, and 32% higher in 2019, 2020, and 2021, respectively, compared to the long-term annual rainfall in the area (close to 320 mm). As an average, the rainfall ranged 20–30 mm more per month during the spring and autumn periods over the three experimental seasons with respect to the typical mean rainfall in the area.

Table 2. A summary of the monthly meteorological means or sums recorded over the three experimental seasons.

Year	Month	T_a (°C)	Hr (%)	u_2 (m s^{-1})	R_n (MJ m^{-2} d^{-1})	R (mm)	ET_o (mm d^{-1}) *
2019	Jan *	7.0	59.1	2.8	3.5	3.0	1.9
	Feb *	8.7	59.1	2.0	6.0	3.6	2.3
	Mar *	11.1	51.8	1.8	7.8	15.0	3.1
	Apr	12.8	65.8	2.2	7.9	136.0	3.1
	May	17.9	57.4	1.7	11.1	23.0	4.9
	Jn	22.1	47.6	1.6	11.7	0.7	6.0
	Jl	25.8	47.1	1.5	11.2	0.0	6.1
	Aug	25.3	56.4	1.2	10.4	14.5	5.3
	Sep	21.1	71.2	1.1	7.4	114.7	3.4
	Oct	16.8	69.9	0.9	5.3	39.0	2.6
	Nov	11.7	64.1	2.3	2.2	24.7	1.8
	Dec	9.9	79.3	1.0	1.5	34.3	1.3
2020	Jan	6.8	77.4	1.8	2.9	69.4	1.2
	Feb	11.0	70.5	1.7	5.7	0.2	2.1
	Mar	10.7	70.8	2.2	5.6	143.8	2.4
	Apr	12.5	75.8	1.3	8.5	62.6	2.9
	May	17.9	63.4	1.3	12.4	53.0	4.5
	Jn	22.3	52.6	1.2	14.2	4.3	5.6
	Jl	25.1	57.0	1.1	14.6	3.8	5.8
	Aug	25.4	50.8	1.0	12.6	0.0	5.5
	Sep	20.2	65.2	1.0	9.2	45.2	3.7
	Oct	14.9	65.0	1.0	5.9	16.0	2.6
	Nov	15.0	64.7	0.3	5.5	120.0	1.3
	Dec	7.7	70.9	2.4	3.0	17.6	1.3

Table 2. *Cont.*

Year	Month	T_a (°C)	Hr (%)	u_2 (m s^{-1})	R_n (MJ m^{-2} d^{-1})	R (mm)	ET_o (mm d^{-1}) *
2021	Jan	6.2	70.3	2.5	3.1	63.3	1.4
	Feb	9.9	76.4	0.8	4.3	5.4	1.9
	Mar	10.7	70.1	1.0	7.4	25.6	2.5
	Apr	12.9	78.2	0.9	9.7	42.0	2.7
	May	18.0	63.2	1.0	14.8	43.8	4.6
	Jn	21.1	66.2	0.9	16.2	23.3	5.1
	Jl	24.5	57.4	0.9	17.5	35.0	6.1
	Aug	24.9	62.3	0.8	13.3	6.6	5.0
	Sep	21.3	72.8	0.7	10.7	119.6	3.5
	Oct	16.9	74.5	0.8	6.7	25.4	2.0
	Nov	10.7	63.9	1.6	3.3	26.9	1.5

T_a: mean daily air temperature; Hr: mean daily relative humidity; u_2: mean daily wind speed measured at 2 m; R_n: mean daily net radiation; R: monthly total rainfall; ET_o: mean daily grass reference evapotranspiration calculated using the FAO56-PM equation; * Data recorded from "Ontur" weather station [38].

3.2. Plant Determination and Soil Water Content Evolution

Overall, both SDI and DI treatments showed a similar crop development, reaching the main crop phenological stages at the same time across the three seasons (Table 3). The duration of the almond crop seasons was 276, 300, and 256 days in 2019, 2020, and 2021, respectively. During the three experimental seasons, almond crop growth was homogenous for the crown diameter (Dc, Appendix A), tree height (Ht, Appendix A), and f_c variables, showing no significant differences between the two treatments (Figure 3). In 2019, the Dc and Ht grow patterns were linear with time, showing an increase of around 1.20 and 1.15 m, respectively (Figure 3a,b). However, the crop growth pattern on Dc and Ht followed a third-order polynomial model during 2020 and 2021 (Figure 3a,b), with a certain stabilization at the end of July (linear and polynomial models not adjusted to Dc data). Thus, the linear growing phase showed an increase of over 1.09 and 0.73 m for Dc and Ht, respectively, in 2020 (values ranging between 2.30–3.38 m for Dc and 2.54–3.26 m for Ht; Figure 3a,b), while the former crop grow rate was about 37% less in 2021 for both variables.

Table 3. The phenological stages of the almond orchard crop over the three growing seasons.

Description of Phenological Stage	BBCH Identification Codes	Phenological Period	Growing Season Date		
			2019	2020	2021
Swollen bud	51	I	19-feb	30-ene	02-feb
Full bloom	65		18-mar	09-mar	15-mar
Fruit set	71	II	26-mar	20-mar	30-mar
Fruit final size/early pit hardening	79		07-may	30-abr	29-abr
Early hull split	85	III	09-ago	10-ago	05-ago
Fruit ripe (harvest)	89	IV	01-sep	28-ago	27-ago
50% of leaves fallen	95		21-nov	25-nov	15-oct

I: from swollen bud to onset of fruit set; II: from onset of fruit set to onset of fruit final size; III: from onset of fruit final size to fruit ripe (harvest crop); IV: from harvest to 50% of leaves fallen.

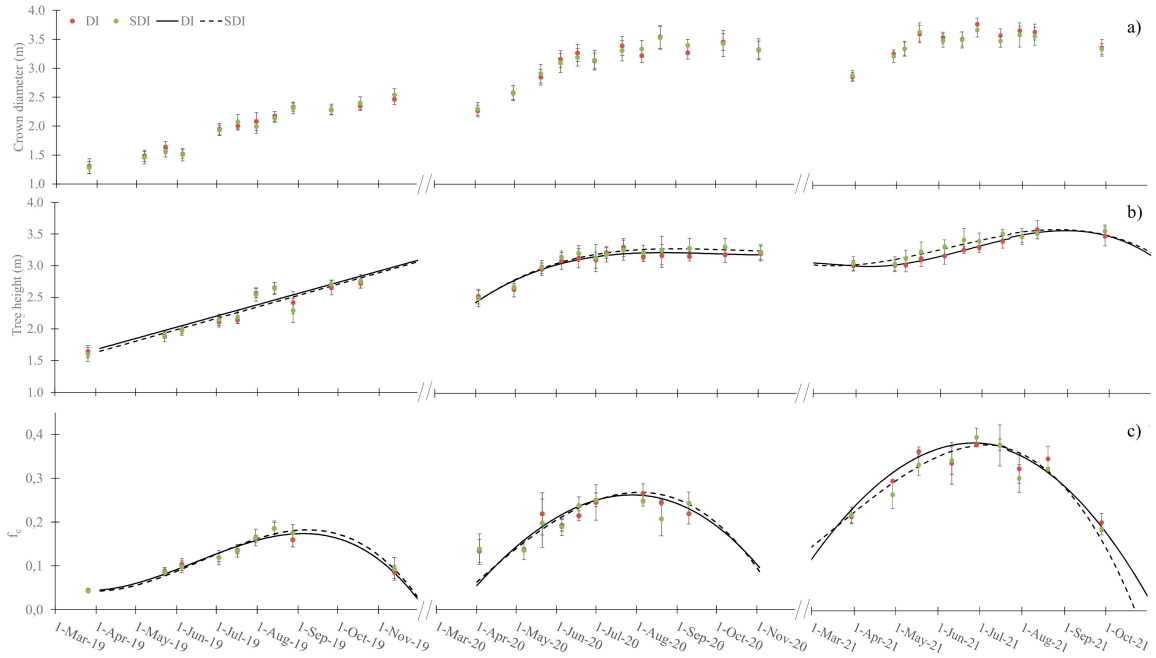

Figure 3. Evolution of the crown diameter (**a**), tree height (**b**), and fraction of ground covered by the canopy (f_c; **c**), for the three growing seasons in both treatments (DI: surface drip irrigation; SDI: subsurface drip irrigation). Vertical error bars represent the standard deviation of the ground sampling for each date and treatment. Continuous and dashed lines superposed to Figure 3b,c correspond to tree height and f_c modeling for the DI and SDI treatments, respectively.

A similar behavior was observed for the f_c variable (i.e., an increase from the onset of each growing season up to end of July or beginning of August), and a descent from then on (Figure 3b). The maximum average f_c values reached 0.19, 0.26, and 0.39 in 2019, 2020, and 2021, respectively, identifying the f_c decline phase after that. Minimum values of the measured f_c were around 0.09 in 2019 and 0.20 in 2021 (Figure 3c), with these data being sampled at a date close to the end of the crop cycle (50% of the leaves fallen; Table 3). Although no ground measurements of f_c were carried out at the end of the growing season in 2020 (Figure 3c), the modeled f_c showed a similar tendency in both treatments, modeling a minimum value of around 0.10 at the end of the second experimental season, which was close to the f_c modeled at the onset of the 2021 season (Figure 3c).

Following the standard practice in the area, irrigation water and fertilizers were applied with almost daily frequency over the three growing seasons (daily irrigation water depth ranged between 1.8 and 6.2 mm), according to the methodology described in Section 2.5. In 2019, the amount of irrigation water applied on the DI treatment was 2581 m^3 ha^{-1}, with 10.0% less applied in the SDI treatment (Table 4). However, the former irrigation amount was duplicated during 2020 (Table 4), applying around 13.9% more irrigation water in the DI than in the SDI treatment. A similar difference (13.7%) between the DI and SDI treatments was determined in the last growing season (2021), increasing the irrigation amount by around 38% with respect to that applied in both treatments during the 2020 season (Table 4). This increase in water applied over the course of the study was mainly due to an increase in tree canopies (i.e., maximum f_c changed from 0.19 in 2019 to 0.39 in 2021).

Table 4. The water applied, yield components, and commercial kernel yield, irrigation water productivity, water use efficiency, and nitrogen productivity for the three years of study.

Season	Treat.	IW (m^3 ha^{-1})	W_k (g)	R_k (%)	Y_k (kg ha^{-1})	IWP (kg m^{-3})	R [1] (m^3 ha^{-1})	Iw[1] (m^3 ha^{-1})	WUE_c [1]	NP (kg kg^{-1})
2019	DI	2581	-	-	-	-	3557	2332	0.44	-
	SDI	2324	-	-	-	-		2076	0.42	-
2020	DI	5188	0.97	29.5	479.8	0.09	658	4089	0.70	5.34
	SDI	4468	0.95	28.7	411.8	0.09		3531	0.74	4.36
	SEM	-	0.01	0.3	33.4	0.01	-	-	-	0.23
	p-value	-	ns	ns	ns	ns	-	-	-	ns
2021	DI	7158	0.84	31.4	2206.4	0.31 a [#]	3530	7060	0.57	13.43
	SDI	6174	0.80	31.1	2163.0	0.35 b		6083	0.48	14.00
	SEM	-	0.01	0.4	59.4	0.01	-	-	-	0.37
	p-value	-	ns	ns	ns	*	-	-	-	ns

Treat.: treatment; IW: total irrigation water applied; W_k: kernel unit weight; R_k: ratio kernel fresh weight vs. in-shell fruit fresh weight; Y_k: commercial kernel yield; IWP: water productivity in terms of irrigation water applied; R: total rainfall for the monitored period; Iw: irrigation amount for the monitored period; WUE_c: water use efficiency in terms of crop evapotranspiration; NP: nitrogen productivity in terms of kernel yield; [1]: data obtained for the monitored period running STSEB model; DI: surface drip irrigation; SDI: sub-surface drip irrigation; SEM: standard error of the mean; [#]: means within a column by different letters are significantly different according to Duncan's test; *p*-value: *: $0.01 < \alpha < 0.05$; ns: not significant.

The irrigation scheduling applied during each growing season, in conjunction with the rainfall events that occurred, allowed for the crop water status to be maintained between −0.5 MPa and −1.1 MPa during the crop growth stage (measurements of midday steam water potential, Ψ_s, from April to the onset of August; Figure 4). However, Ψ_s was much lower (around −1.5 MPa) during the period close to harvest time in the 2020 and 2021 experimental seasons, being a common farming practice to reduce irrigation during that period in order to minimize the risk of bark splitting. After harvesting, the crop water status of both treatments recovered toward Ψ_s higher than −1.0 MPa (Figure 4). Overall, Ψ_s showed no significant differences between the two treatments.

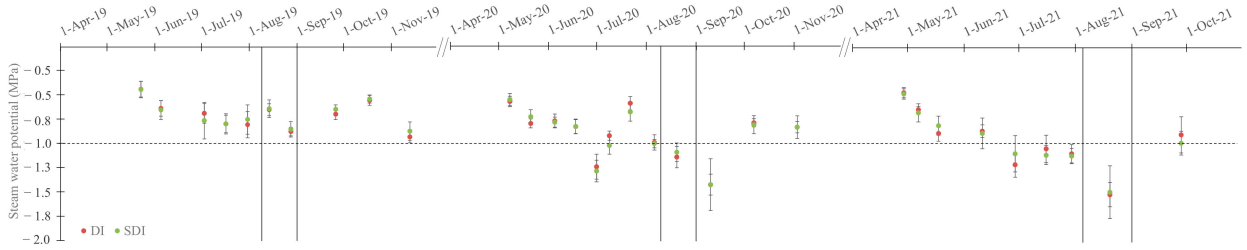

Figure 4. Evolution of the midday steam water potential (Ψs; MPa) for the three growing seasons. Vertical lines show the period between early hull split and harvest. Horizontal dashed line shows the threshold of tree water stress [44]. Vertical error bars represent the standard deviation of the measurements for each date and treatment.

The daily volumetric soil water content measured in both treatments showed a similar evolution over each growing season, with both curves moving between field capacity (FC, Appendix A) and permanent wilting point (PWP, Appendix A) (Figure 5). Although both curves showed the same trend, the SDI curve was 3.1% lower than that of the DI, as an average, being stressed in the 2021 season (around 4.2% difference; Figure 5). Some heavy rainfall events (between 35 and 70 mm of precipitation) that occurred during spring and autumn of the three seasons contributed to increasing the soil water content toward values close to FC or higher. However, during the end of spring and up to the fruit ripening stage, irrigation events were the main water contribution to the crop since rainfall events were scarce. The minimum soil moisture values of both treatments were measured at days close to harvest time, except for the first experimental season, when the almond crop was not harvested. These values ranged between 0.17 and 0.20 m^3 m^{-3}.

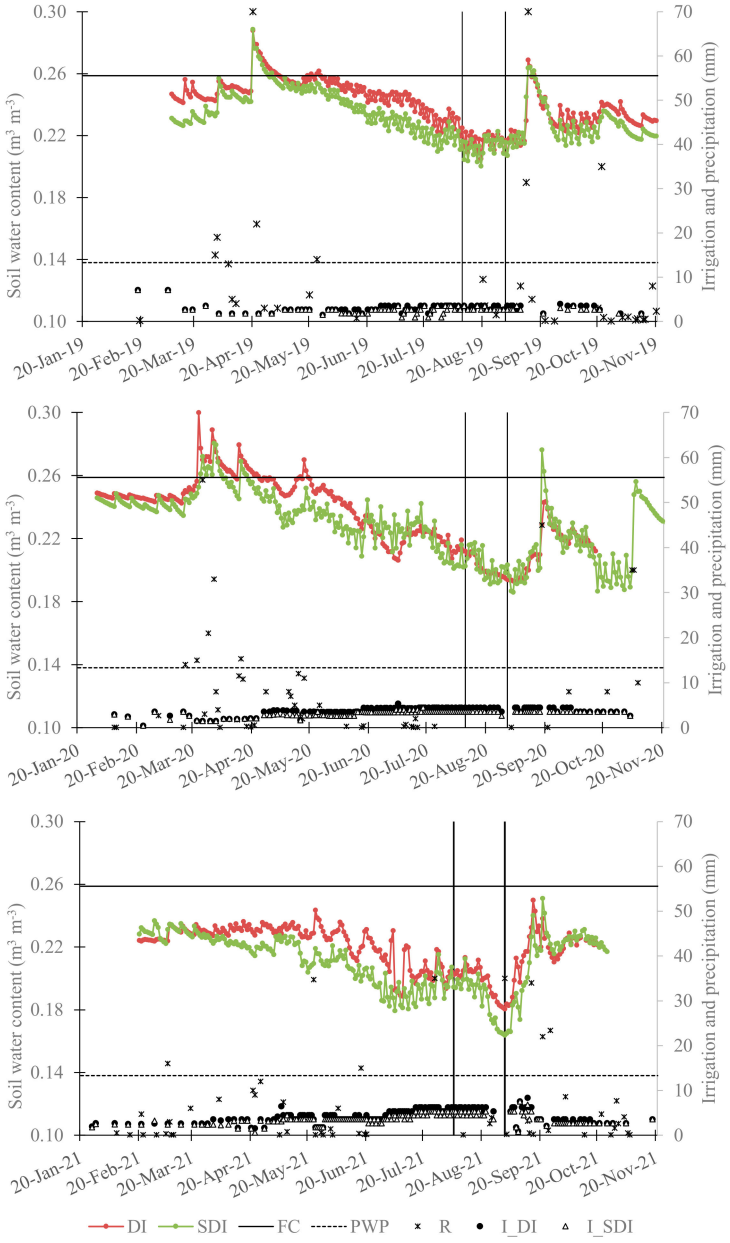

Figure 5. The daily soil water content evolution for the three growing seasons in both treatments (DI: surface drip irrigation; SDI: sub-surface drip irrigation). Vertical lines show the period between early hull split and harvest. Continuous and dashed horizontal lines are the field capacity (FC) and permanent wilting point (PWP), respectively. The irrigation and precipitation depths are also plotted.

3.3. Almond ET_c Estimations Using the STSEB Model

The daily ET_c values and T_c/E_s partition obtained by the STSEB model, together with the available thermal infrared data, were constrained to 251 days in 2019 (from 4 April to 12 December), reduced to 152 days in 2020 (from 5 June to 3 November) due to the pandemic situation, and to 286 days in 2021 (from 18 February to 30 November). These monitored periods were not sufficient to derive the seasonal ET_c values, except for the last growing season, which did cover almost the full phenological development of the almond trees (Table 3).

The evolution of the daily ET_c and T_c values showed a rising trend during both each growing season and between the three experimental seasons (Figure 6), mainly due to the development of the tree canopies, thanks to favorable spring–summer temperatures and the older age of the trees. The maximum mean daily ET_c values were reached from June

to August (coinciding with the highest evaporative demand and the kernel-filling stage; Figure 6; Table 3) ranging between 1.3 and 1.4 mm day^{-1} in 2019, 2.6–2.9 mm day^{-1} in 2020 and between 3.2 and 4.5 mm day^{-1} in 2021 (Figure 6). The mean ET_c values ranged from 0.5 mm day^{-1} (onset and fall of crop growth cycle) to 2.2 mm day^{-1} (crop development and post-harvest period) during the rest of the monitored period (Figure 6).

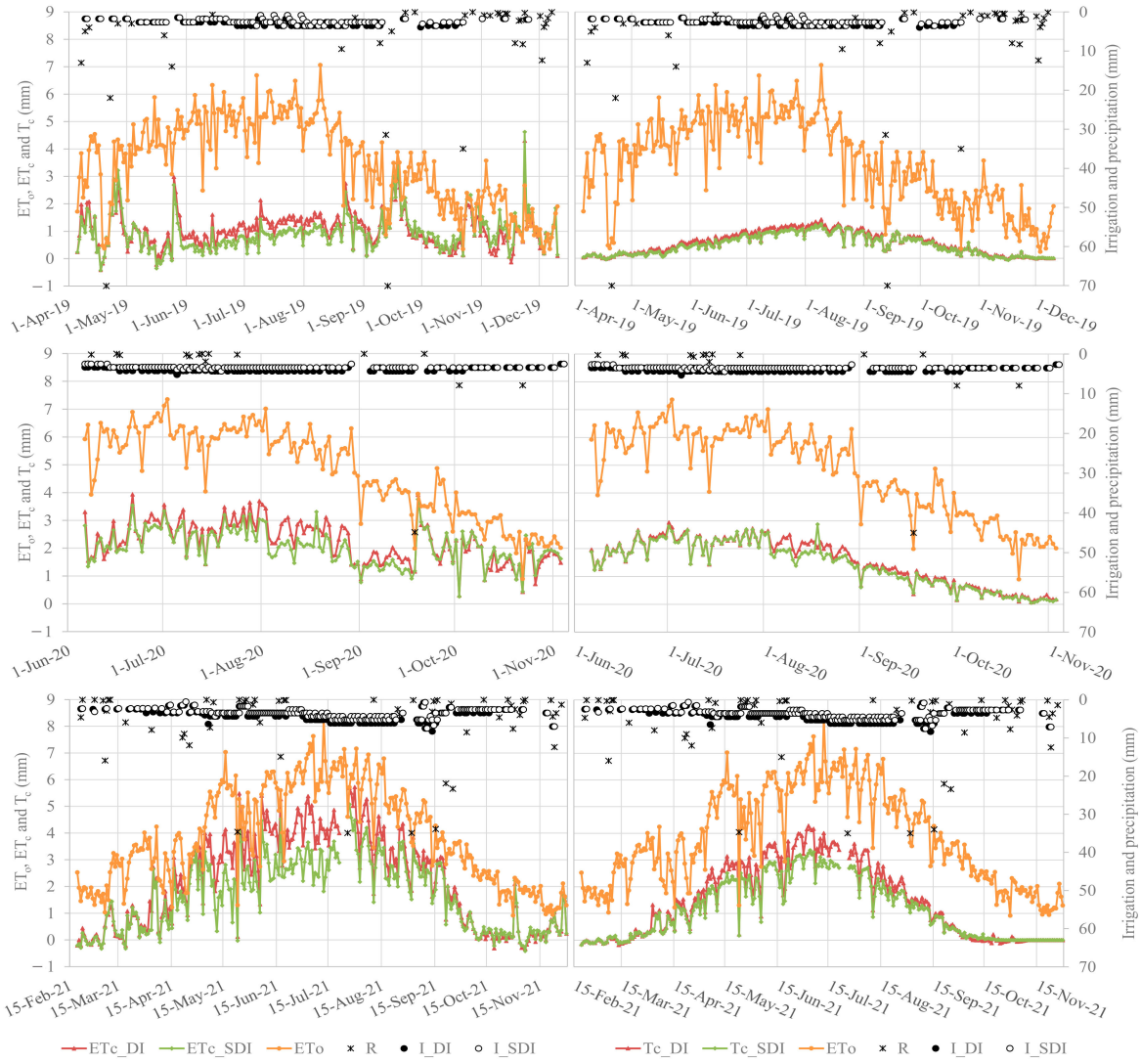

Figure 6. The daily evolution of the crop evapotranspiration (ET_c; captions on the left) and crop transpiration (T_c; captions on the right) for the three growing seasons in both treatments (DI: surface drip irrigation; SDI: sub-surface drip irrigation). The crop reference evapotranspiration (ET_o), irrigation and precipitation are also plotted.

In terms of T_c, the maximum values were also obtained during the highest ET_o period (May–August; Figure 6). The maximum mean daily T_c values were 15–20% lower in 2019 and 2020, and up to 35% lower in 2021 than the ET_c values for the DI treatment, while these differences were 7% (2019), 12% (2020), and 19% (2021) lower for T_c than ET_c in the SDI treatment. Overall, the accumulated ET_c was relatively close between treatments for the 2019 and 2020 seasons (differences of 25.9 mm and 27.9 mm, respectively; Figure 7) and a large difference in ET_c accumulated was estimated in 2021 (138.5 mm; Figure 7). With respect to soil evaporation (E_s), the STSEB model was able to differentiate this component between the two irrigation systems, estimating 5.6 mm, 27.9 mm, and 45.2 mm less E_s in the SDI treatment than in the DI treatment during the monitored periods of 2019, 2020, and 2021, respectively (Figure 7).

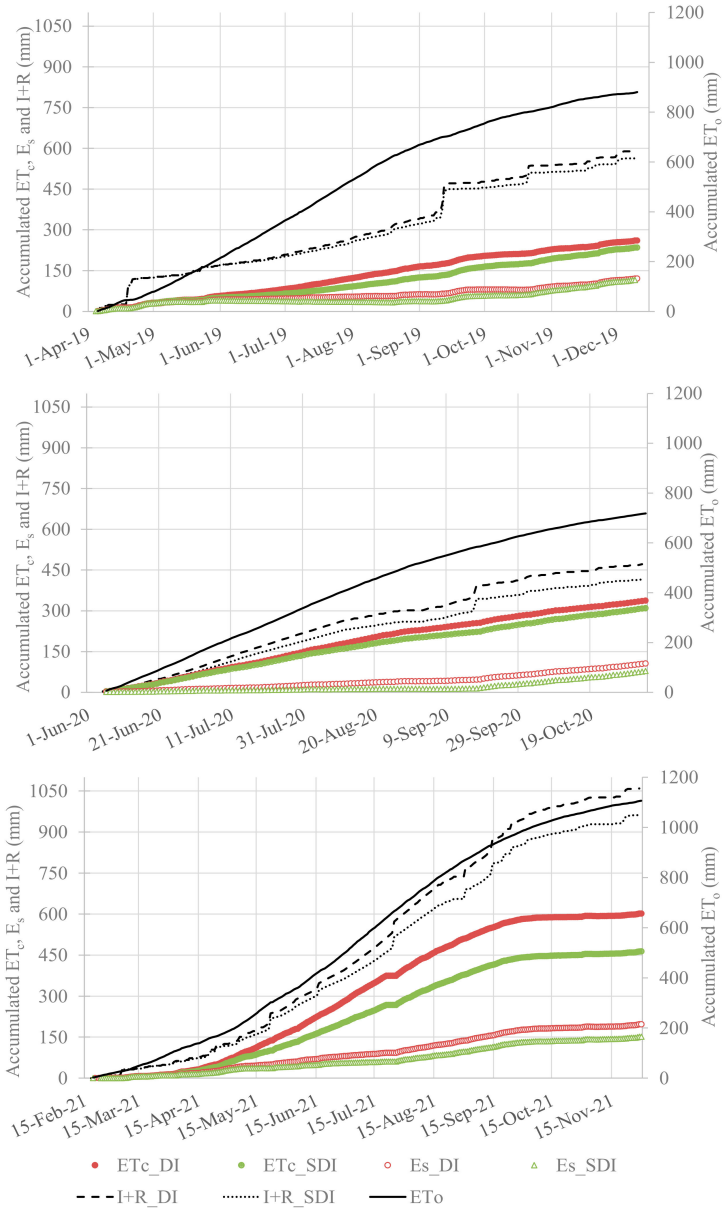

Figure 7. The seasonal evolution of accumulated ET_c and E_s estimations using the STSEB approach for the three growing seasons in both treatments (DI: surface drip irrigation; SDI: sub-surface drip irrigation). ET_o and irrigation plus precipitation (I + R) are also represented.

3.4. Plant–Water Relations

The field dataset gathered allowed us to derive some plant–water relations for both treatments. Thus, the measured daily soil water content and the estimated daily crop transpiration were related to the daily data of crop water status (Ψ_s; Figure 8). Ψ_s values and their evolution (Figure 4) for the three growing seasons were in line with the measured soil moisture data (Figure 5), where the soil moisture dropping off between 0.18 and 0.20 m^3 m^{-3} caused the highest crop water deficit ($\Psi_s < -1.15$ MPa; Figure 8a). A clear correlation was found between soil moisture and Ψ_s, obtaining coefficients of determination of 0.60 and 0.52 for the DI and SDI treatments, respectively (Figure 8a). A similar trend was identified between T_c and Ψ_s during the kernel-filling period (from June to August) of the two last growing seasons (Figure 8b), where T_c was shortened around 45% in 2020 and between 21% (for DI treatment) and 31% (for SDI treatment) in 2021 when Ψ_s declined from −1.1 MPa to −1.5 MPa. No evidence was reported for 2019 (Figure 8b).

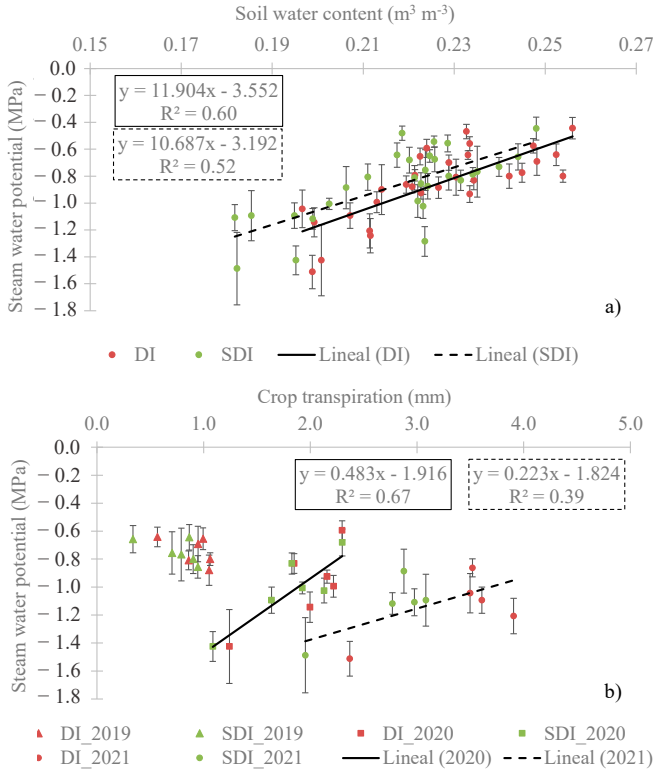

Figure 8. The relationship between (**a**) the daily soil water content and the midday steam water potential and (**b**) the daily crop transpiration and the midday steam water potential during the three growing seasons in both treatments (DI: surface drip irrigation; SDI: sub-surface drip irrigation). Vertical error bars represent the standard deviation of the mean values of eight determinations.

3.5. Almond Yield Response to Irrigation Systems, Water, and Nitrogen Productivities and Water Use Efficiency

The almond crop harvest was obtained for the second and third experimental year. In both growing seasons, neither yield components (W_k and R_k) nor kernel yield showed significant differences between the irrigation systems (Table 4). Standard commercial kernel yields (Y_k, 7% moisture content) obtained in 2020 and 2021 were around 446 kg ha^{-1} and 2185 kg ha^{-1}, respectively (Table 4). The kernel unit weight (W_k) was, as average data, 0.94 g for 2020 and 0.82 g for 2021, while the kernel fraction (R_k) was 29.1 and 31.3% in 2020 and 2021, respectively. The calculated irrigation water productivity (IWP) was 0.09 kg m^{-3} as the average value for both treatments in 2020 (Table 4). This value was multiplied by almost 5 in both treatments for 2021, when the SDI treatment showed a significantly higher value (0.35 kg m^{-3}) than the DI treatment (0.31 kg m^{-3}; Table 4).

Constraining the analysis to the period with available thermal infrared measurements for running the STSEB model, the water use efficiency in terms of ET_c (WUE_c) showed that close to 50% of water applied in 2019 and 2021 and around 72% of that in 2020 was consumed through the evapotranspiration process, reaching values of 0.44, 0.70, and 0.57 in the DI treatment, and 0.42, 0.74, and 0.48 in the SDI treatment for 2019, 2020, and 2021, respectively (Table 4). Finally, the irrigation systems showed no significant differences with respect to the computed nitrogen productivity (NP) values for the last two experimental years, obtaining average values of 4.85 kg kgN^{-1} in 2020 and 13.7 kg kgN^{-1} in 2021 (Table 4).

4. Discussion

4.1. Effects of Irrigation System on Crop Growth and Development

In general, the almond crop growth and development was not limited by a lack of available water for the entire experimental period, since the almond trees showed a suitable

water status, with the exception of some specific moments and before harvesting, when the trees were medium to moderately stressed, following Fulton et al. [44] ($\Psi_s \leq -1.0$ MPa; Figure 4). This was especially significant over the first growing season, and during the crop growth periods (from swollen bud to early hull split; Table 3) for the third and fourth crop-greening. The combination of rainfall and irrigation events provided to the crop over the three experimental seasons, together with the fertilizing and pruning schedule, and with a suitable pest and disease program, allowed for fast crop growth and the early onset of the productive period. This can be noted by an important leap in the crop growth evolution, with an increase of around 2.2 and 1.9 m in the crown diameter and tree height, respectively, duplicating the maximum f_c attained by the crop between the 2019 and 2021 growing seasons (Figure 3). Similar patterns of f_c evolution were reported by Espadafor et al. [52], who reported a final f_c value of 0.35 in the fourth crop-greening. Close values of ground cover were also measured by Drechsler et al. [18], reporting values of 0.22 and 0.55 of f_{IPAR}, which were similar to f_c when measured at noon, in the 4- and 5-year-old almond orchards grown in California. Zhang et al. [53] obtained no statistical differences in the f_c evolution of young pomegranate trees irrigated under the DI and SDI systems, although larger f_c values were observed in SDI trees than in DI trees. A field experiment in young peach trees obtained significant differences in f_c between the DI and SDI systems, while both treatments produced larger trees than those irrigated by a microjet (micro-sprinkler) system [54].

Focusing on almond development, although no significant differences between treatments were observed for any experimental season, the inter-season differences in the crop cycle duration (between 25 and 50 days) were mainly generated by the onset date and fall date of each growing season (Table 3). A shorter crop cycle duration in 2021 was due to the improper leaf application of micronutrients a few weeks after harvest, which caused leaf fall to move forward (Table 3). The date of the rest of the phenological stages were close between seasons (between 3 and 10 days), with these inter-season differences shortening toward fruit maturity (early hull split and fruit ripe; Table 3). In addition, the full bloom stage of this study with the 'Penta' cultivar (Table 3) is consistent with that reported by Lorite et al. [55] for late-flowering cultivars ('Lauranne' and 'Marta').

4.2. Effects of Irrigation System on Crop and Soil Water Status

The lowest Ψ_s values measured in both treatments (around -1.5 MPa; Figure 4), considered as mild to moderate stress [44], were obtained at dates close to crop harvest (points close to vertical lines in 2020 and 2021; Figure 4). A lower irrigation frequency was the main reason for these values, the aim of which was to give a higher lignification level to the main stem tree and avoid bark damage with the inverter-umbrella type fruit collecting machine. A similar behavior of crop water status, although much more pronounced, was observed by Drechsler et al. [18] during almond harvest activities, reporting between -2.0 and -3.1 MPa at the end of August in 3- and 4-year-old orchards. Regarding the crop water relations obtained (Figure 8), similar results were also reported by Espadafor et al. [56], who determined that T_c could reach up to a 45% of difference when Ψ_s declined up to -1.6 MPa.

Considering the soil moisture evolution (Figure 5), a similar pattern to that measured by Ψ_s was also observed, measuring the lowest soil water content around harvest period during the two last growing seasons. However, consistent soil water depletion between the first and the last growing seasons, and between both treatments, was identified by the soil moisture sensors. The increase in f_c between both seasons could result in a higher rainfall interception by the canopy, causing an improper capture of the soil moisture level by the soil sensor probes, already located under canopy cover in the third growing season (Figure 5). In a practical and operative sense, the trends shown in Figure 8a should be used with caution, since soil moisture content represents one point of the soil, close to the drip line, and does not integrate the real soil moisture content for the tree spacing.

4.3. Effects of Irrigation System on ET_c and Its Partition

Analyzing the effect of the irrigation system on the almond ET_c estimates and their partitions (E_s and T_c), minor differences (between 0.1–0.2 mm day^{-1}) were determined on a daily basis between the DI and SDI treatments for the spring and fall periods in the three experimental years (Figure 6). Differences emerged during the higher ET_o period (from May to August; Figure 6), resulting in being up to 1.0–1.3 mm day^{-1} higher for the DI treatment than the SDI treatment in ET_c for the last growing season (Figure 6). Considering the estimated T_c, very close values for both treatments were estimated during the three growing seasons (Figure 6) since the f_c evolution was similar for both treatments (Figure 3c). A slightly higher f_c in DI than in SDI during April–July for the last season (between 0.5–2.4% more of f_c; Figure 3c) generated the largest differences in T_c, ranging from 0.3–0.6 mm day^{-1} higher for the DI than for the SDI treatment (Figure 6). The mean daily ET_c and T_c values derived from the STSEB model (Figure 6) showed a rising trend linked to the increase in f_c across the three experimental years (Figure 3c), as previously identified by Espadafor et al. [52], Drechsler et al. [18], or Sánchez et al. [28], who used different approaches to measure crop evapotranspiration in young almond orchards. Espadafor et al. [52] measured the maximum T_c values of 1.0, 2.5, and 3.1 mm in the second to fourth crop-greening of an almond orchard with a f_c evolution similar to the present experiment. Lower values of ET_c and T_c (up to 3.0 and 2.5 mm day^{-1}, respectively) were obtained by Sánchez et al. [28] in an almond orchard whose maximum f_c was around 0.40. In contrast to the former data, Drechsler et al. [18] reported the maximum mean ET_c values of around 3.0 mm day^{-1} in a 2-year-old orchard and between 7.0 and 8.0 mm day^{-1} in 3- and 4-year old orchards, which doubled our ET_c estimations (Figure 6). A feasible explication for these large differences might be the different soil water evaporation rates in the micro-sprinkler irrigated orchards [18] compared to drip-irrigated orchards (either this experiment or those by Espadafor et al. [52] and Sánchez et al. [28]), since the measured f_c data in all of the experiments were in the same range.

Although the SDI lateral irrigation lines were buried 0.35 m below the soil surface, the irrigation management (frequency of irrigation events and water depths) applied to the SDI treatment was intended to eliminate soil evaporation. Note that around 76% less E_s was estimated in the SDI treatment than in the DI treatment (Figure 7) during the periods when the precipitation was null or minimum (June to August, Figure 6). However, the mean daily E_s values were similar between treatments (0.8 and 1.3 mm day^{-1}) for those periods with rainfall events. Burying lateral irrigation lines much deeper, between 0.50 and 0.55 m [32,53], could improve the consumptive water use by the crop since there was still a 24% margin to reduce soil evaporation in the SDI with respect to the DI treatment.

Overall, the accumulated E_s/ET_c ratios were similar between treatments for the three monitored seasons (around 48, 29 and 33% in 2019, 2020, and 2021, respectively), although these values were considerably different between the three monitored periods. Comparing the former ratios for the first and the last growing seasons, where the monitored periods covered almost all the crop growth period (Figure 6), a higher E_s/ET_c ratio was estimated in 2019 than in 2021 (15% more). This difference is explained by the increase in f_c, reducing the potential evaporation from the soil surface. Unlike our results, Bryla et al. [54] found an approximate 10% loss of water to evaporation when the crop was young and the ground surface was not completely shaded. In contrast, Sánchez et al. [28] reported E_s/ET_c ratios (26%) close to our findings and larger than those reported by other authors [53,54].

With respect to the seasonal water use, the accumulated ET_c for the DI and SDI treatments over the three growing seasons were completely covered with the accumulated irrigation and rainfall, being between 25 and 50% over the accumulated ET_c (Figure 7). The main reason was the rigorous fertigation program implemented each season by the grower, where a daily dose fertilization had to be applied to the crop, regardless of the rainfall. Thus, around 0.80 h day^{-1} was the minimum irrigation period used when a moderate-heavy rain took place. Although this was a limitation in improving the rainwater use efficiency, not considering rainfall events in the accumulated calculations allowed us to determine that

the irrigation amount applied to each monitored season and treatment were close to the accumulated ET_c (Table 4; Figure 7).

4.4. Effects of Irrigation System on Yield, Use of Water and Nitrogen

The Y_k for 2021 increased around 5 times compared to that harvested in 2020, attaining a mean value of 2206 and 2163 kg ha^{-1} for the DI and SDI treatments, respectively (Table 4). These values were hardly ever reached in the area with a 4-year-old almond orchard, whose Y_k was close to those obtained in mature trees grown under similar climatic conditions [10,57–60], although somewhat distant from the maximum kernel yields obtained in southern San Joaquin Valley (over 4400 kg ha^{-1}; [44,61]). The significant increase in Y_k caused the yield components to be compensated for, obtaining mean W_k and R_k values were around 14.6% lower and 7.2% higher, respectively, in 2021 vs. 2020 (Table 4). The measured W_k data in this research (0.96 and 0.83 g) were comparatively lower than those reported in other works, which ranged between 1.26 and 1.05 g [10], around 1.18 g [34] or between 1.27 and 1.59 g [57]. The agronomic characteristics of each cultivar used in those experiments ('Guara', 'Cartagenera', and 'Marta' vs. 'Penta') are the main reason for these differences. However, our R_k data were similar to the kernel fraction obtained by Egea et al. [57] and Romero et al. [34].

A 13.7% less of the seasonal irrigation amount (IW) applied in the SDI treatment vs. DI treatment for 2021 allowed for the irrigation water productivity (IWP) of SDI to be significantly improved in 0.04 kg m^{-3} (12.9% higher) with respect to that calculated in the DI treatment (0.31 kg m^{-3}; Table 4). However, a non-significant increase in IWP was observed for 2020, since 14.2% less of Y_k in the SDI vs. DI was compensated for by the lower IW applied (13.9%), obtaining the same IWP in both treatments (Table 4). Despite the almond trees in the third and fourth crop-greening being at the training phase, a lower Y_k was obtained in 2020 compared to that in 2021 because of the different f_c values reached by the orchard (Figure 3c). The increase in IWP for SDI for 2021 was mainly justified by the lower evaporation losses from soil and the easy availability of water within the root zone [19,29]. Similar improvements in IWP were reported by Ayars et al. [32] and Ma et al. [33], who achieved between 6.5 and 14.7% more IWP for the SDI system than the DI system in pomegranate and vines, respectively. The IWP values computed for 2021 were close to those reported by several authors in mature almond orchards managed under full irrigation [10,59,60], whose data ranged between 0.25 and 0.40 kg m^{-3}.

The WUE_c data for both treatments in 2020 showed that around 28% of the water applied corresponded to non-beneficial water use (N-BWU) (i.e., water lost through deep percolation and runoff) [4,45]. However, higher percentages of N-BWU were computed for 2019 (around 57%) and 2021 (among 43% for DI treatment and 52% for SDI treatment). These differences in percentages between experimental seasons may be explained by the length of the monitored period in 2020, which covered both the summer and fall periods, with a lower precipitation amount than those values reported for 2019 and 2021 (65.8 vs. 354 mm; Table 4). From this analysis and those related to seasonal water use (Figure 7), we may deduce that in both irrigation management schedules, in combination with the rainfall events, a proper soil water reservoir was maintained over the three growing seasons, allowing for similar tree growth and development as well as plant–water status. As a result of these findings, and the almond orchard management implemented, a fast onset of the productive period for young trees was achieved, as proven by the Y_k obtained.

Finally, the computed nitrogen productivity (NP) values showed no differences between the two irrigation systems for the two last experimental years despite some minor differences observed (Table 4). A significant increase in this indicator was noted in both treatments, with these values in 2021 being around 2.9 times higher than those computed in 2020 (Table 4). Ayars et al. [32] reported higher NP in the SDI than in the DI treatment in two of the three experimental seasons studied. However, these authors determined a decrease in each experimental season with increasing levels of nitrogen applied, since there was no yield increase associated with the increased levels of applied N. A similar

behavior might be occurring in the almond trees, and this will be further explored in coming growing seasons.

5. Conclusions

The results of this research show that both almond crop growth and development as well as the almond tree water status showed no significant differences between the two different drip-irrigation systems (surface, DI; and subsurface, SDI) over three growing seasons in a young almond orchard. In terms of crop-water use (ET_c and its partition, E_s and T_c) estimated from the two-source energy balance modeling (STSEB), trees under both treatments showed minor differences for the spring and fall periods (0.1–0.2 mm day^{-1}), while larger differences (1.0–1.3 mm day^{-1} of ET_c higher for DI treatment than SDI treatment) were obtained during more demanding ET_o periods. Nevertheless, crop transpiration (T_c) was similar in both treatments during the three monitored periods, with maximum values increasing with f_c development. Additionally, soil evaporation (E_s) was influenced by the increase in f_c over the three growing seasons, being around 48% in 2019 and 33% in 2021.

The irrigation management applied in both treatments during the study period allowed us to guarantee both a proper soil water level and a suitable crop-water status during the young-almond phase. Good correlations were obtained between the steam water potential and both soil moisture and crop transpiration. In addition, to manage the almond orchard under pristine conditions (well-managed fertigation, pest and diseases, and training system) generates a fast onset of the productive period. A reduction of between 10% and 13.8% in the seasonal irrigation amount applied in the SDI with respect to the DI, generated good tree performance, since no differences were found between the two irrigation systems in either yield components or in the kernel yield resulted. However, significant differences between treatments were obtained in terms of irrigation water productivity for the last experimental season, resulting in being 12.9% higher for the SDI than the DI treatment. No significant differences between the treatments were found for nitrogen productivity. These encouraging results suggest that the SDI system could be a sustainable alternative to reduce consumptive water use and to increase the water productivity in almond orchards, a crop with high crop water requirements traditionally planted in areas with limited water resources.

Author Contributions: Conceptualization, R.L.-U., J.G.-P. and J.M.S.; Methodology, R.L.-U., F.M. and J.M.S.; Software, F.M. and J.M.S.; Validation, F.M. and R.L.-U.; Formal analysis, F.M., J.M.S. and R.L.-U.; Investigation, R.L.-U., J.G.-P., F.M. and J.M.S.; Resources, R.L.-U., J.G.-P. and J.M.S.; Data curation, F.M.; Writing—original draft preparation, F.M.; Writing—review and editing, R.L.-U., J.G.-P. and J.M.S.; Visualization, R.L.-U.; Supervision, R.L.-U. and J.M.S.; Project administration, R.L.-U., J.G.-P. and J.M.S.; Funding acquisition, R.L.-U., J.G.-P. and J.M.S. All authors have read and agreed to the published version of the manuscript.

Funding: This research was funded by the "Consejería de Educación, Cultura y Deportes"of Castilla-La Mancha, Spain, with FEDER co-financing, project SBPLY/17/180501/000357 and the APC was funded by project PID2020-113498RB-C21 under "Agencia Estatal de Investigación", Spain, together with FEDER funds.

Institutional Review Board Statement: Not applicable.

Informed Consent Statement: Not applicable.

Data Availability Statement: Not applicable.

Acknowledgments: The authors would like to thank José Joaquín Sánchez for letting them work on the almond orchard and for providing them with all of the necessary information during the experimental campaigns. His kindness is much appreciated. R. López-Urrea expresses his gratitude for the support from the European Commission and PRIMA program with project "SUPROMED" (grant number: 1813). The work of J. M. Sánchez and J. González-Piqueras was supported by H2020 EC project "REXUS" under grant 101003632.

Conflicts of Interest: The authors declare no conflict of interest.

Appendix A

Abbreviations	Units	Meaning
ANOVA	-	Analysis of variance
Dc	m	Crown diameter
DI	-	Surface drip irrigation system
$D_{r,i}$	mm	Soil water depletion
DRZ	-	Direct root zone irrigation
E_s	mm	Soil evaporation
ET_c	mm	Crop evapotranspiration
ET_o	mm	Reference crop evapotranspiration
f_c	fraction of unity	fraction of ground covered by the canopy
FC	$m^3\ m^{-3}$	Field capacity
f_{IPAR}	fraction of unity	fraction of intercepted photosynthetic active radiation
F_u	kg $tree^{-1}$	Total in-shell fruit fresh weight per tree
G	W m^{-2}	Soil heat flux
H_{Ff}	%	Water content of fruit fresh weight
Hr	%	Mean daily relative humidity
H	W m^{-2}	Sensible heat flux
Ht	m	Tree height
I	mm	Irrigation depth
IRT	-	InfraRed Thermometers
IW	$m^3\ ha^{-1}$	Seasonal irrigation water applied
IWP	kg m^{-3}	Irrigation Water Productivity
K_{cb}	addimensional	Standard basal crop coefficient
$K_{cb\ end}$	addimensional	Kcb for end season
$K_{cb\ ini}$	addimensional	Kcb during initial crop stage
$K_{cb\ mid}$	addimensional	Kcb during mid-season stage
K_d	addimensional	density coefficient
LE	W m^{-2}	Surface latent heat flux
LE_c	W m^{-2}	Canopy latent heat flux
LEs	W m^{-2}	Soil latent heat flux
N-BWU	-	Non-beneficial water use
NP	kg kg^{-1} N	Nitrogen productivity
PAR	-	Photosynthetically active radiation
P_e	mm	effective precipitation
PWP	$m^3\ m^{-3}$	Permanent Wilting Point
R	mm	Monthly total rainfall
RAW	mm	Readily available water
RDI	-	Regulated deficit irrigation
REW	mm	Readily evaporative water
R_k	fraction of unity	Kernel fraction
R_n	W m^{-2}	Net radiation flux
SDI	-	Subsurface drip irrigation system
SEB	-	Surface energy balance
STSEB	-	Simplified Two-Source Energy Balance
SWB	-	Soil water balance
T_a	°C	Mean daily air temperature
T_c	mm	Crop transpiration
Td	plants ha^{-1}	Tree density
TEW	mm	Total evaporable water
u2	m s^{-1}	Mean daily wind speed
W_k	g	Kernel unit weight
WUEc	mm mm^{-1}	Crop-water use efficiency
Y_k	kg ha^{-1}	Commercial kernel yield
Ze	m	Depth of the evaporative soil layer
Zr	m	Depth of the root zone layer
λ	J kg^{-1}	Latent heat of vaporization of water
Ψ_s	MPa	Midday steam water potential

References

1. O'Connor, B.; Moul, K.; Pollini, B.; de Lamo, X.; Simonson, W. *Earth Observation for SDG Compendium of Earth Observation Contributions to the SDG Targets and Indicators*; ESA: Harwell, UK, 2020; p. 165.
2. FAOSTAT. Food and Agriculture Organization of the United Nations. Stadistic Division. Available online: http://www.fao.org/faostat/en/#home (accessed on 18 June 2022).

3. IPCC. *Climate Change 2022. Impacts, Adaptation and Vulnerability; Intergovernmental Panel on Climate Change*; Cambridge University Press: Cambridge, UK, 2022; p. 3676.
4. Jovanovic, N.; Pereira, L.S.; Paredes, P.; Pôças, I.; Cantore, V.; Todorovic, M. A Review of Strategies, Methods and Technologies to Reduce Non-Beneficial Consumptive Water Use on Farms Considering the FAO56 Methods. *Agric. Water Manag.* **2020**, *239*, 106267. [CrossRef]
5. Pereira, L.S.; Cordery, I.; Iacovides, I. *Coping with Water Scarcity. Addressing the Challenges*, 1st ed.; Springer: Dordrecht, The Netherlands, 2009; ISBN 978-1-4020-9578-8.
6. Perry, C.; Steduto, P.; Karajeh, F. *Does Improved Irrigation Technology Save Water? A Review of the Evidence*; Regional Initiative on Water Scarcity for the Near East and North Africa; Food and Agriculture Organization of the United Nations: Cairo, Egypt, 2017; p. 57.
7. Lorite, I.J.; Ruiz-Ramos, M.; Gabaldón-Leal, C.; Cruz-Blanco, M.; Porras, R.; Santos, C. Water Management and Climate Change in Semiarid Environments. In *Water Scarcity and Sustainable Agriculture in Semiarid Environment*; Elsevier: Amsterdam, The Netherlands, 2018; pp. 3–40. ISBN 978-0-12-813164-0.
8. Goldhamer, D.A.; Viveros, M.; Salinas, M. Regulated Deficit Irrigation in Almonds: Effects of Variations in Applied Water and Stress Timing on Yield and Yield Components. *Irrig. Sci.* **2006**, *24*, 101–114. [CrossRef]
9. Egea, G.; Nortes, P.A.; Domingo, R.; Baille, A.; Pérez-Pastor, A.; González-Real, M.M. Almond Agronomic Response to Long-Term Deficit Irrigation Applied since Orchard Establishment. *Irrig. Sci.* **2013**, *31*, 445–454. [CrossRef]
10. Moldero, D.; López-Bernal, Á.; Testi, L.; Lorite, I.J.; Fereres, E.; Orgaz, F. Long-Term Almond Yield Response to Deficit Irrigation. *Irrig. Sci.* **2021**, *39*, 409–420. [CrossRef]
11. García Tejero, I.F.; Moriana, A.; Rodríguez Pleguezuelo, C.R.; Durán Zuazo, V.H.; Egea, G. Sustainable Deficit-Irrigation Management in Almonds (*Prunus dulcis* L.). In *Water Scarcity and Sustainable Agriculture in Semiarid Environment*; Elsevier: Amsterdam, The Netherlands, 2018; pp. 271–298. ISBN 978-0-12-813164-0.
12. Allen, R.; Pereira, L.; Raes, D.; Smith, M. *Crop Evapotranspiration-Guidelines for Computing Crop Water Requirements*; FAO Irrigation and Drainage Paper 56; FAO: Rome, Italy, 1998; p. 300.
13. Pereira, L.S.; Paredes, P.; Jovanovic, N. Soil Water Balance Models for Determining Crop Water and Irrigation Requirements and Irrigation Scheduling Focusing on the FAO56 Method and the Dual Kc Approach. *Agric. Water Manag.* **2020**, *241*, 106357. [CrossRef]
14. Allen, R.G.; Tasumi, M.; Trezza, R. Satellite-Based Energy Balance for Mapping Evapotranspiration with Internalized Calibration (METRIC)—Model. *J. Irrig. Drain Eng.* **2007**, *133*, 380–394. [CrossRef]
15. Norman, J.M.; Kustas, W.; Humes, K. A Two-Source Approach for Stimating Soil and Vegetation Energy Fluxes from Observations of Directional Radiometric Surface Temperature. *Agric. For. Meteorol.* **1995**, *77*, 263–293. [CrossRef]
16. Pôças, I.; Calera, A.; Campos, I.; Cunha, M. Remote Sensing for Estimating and Mapping Single and Basal Crop Coefficientes: A Review on Spectral Vegetation Indices Approaches. *Agric. Water Manag.* **2020**, *233*, 106081. [CrossRef]
17. Sánchez, J.M.; López-Urrea, R.; Valentín, F.; Caselles, V.; Galve, J.M. Lysimeter Assessment of the Simplified Two-Source Energy Balance Model and Eddy Covariance System to Estimate Vineyard Evapotranspiration. *Agric. For. Meteorol.* **2019**, *274*, 172–183. [CrossRef]
18. Drechsler, K.; Fulton, A.; Kisekka, I. Crop Coefficients and Water Use of Young Almond Orchards. *Irrig. Sci.* **2022**, *40*, 379–395. [CrossRef]
19. Valentín, F.; Nortes, P.A.; Domínguez, A.; Sánchez, J.M.; Intrigliolo, D.S.; Alarcón, J.J.; López-Urrea, R. Comparing Evapotranspiration and Yield Performance of Maize under Sprinkler, Superficial and Subsurface Drip Irrigation in a Semi-Arid Environment. *Irrig. Sci.* **2020**, *38*, 105–115. [CrossRef]
20. Sánchez, J.M.; López-Urrea, R.; Rubio, E.; Caselles, V. Determining Water Use of Sorghum from Two-Source Energy Balance and Radiometric Temperatures. *Hydrol. Earth Syst. Sci.* **2011**, *15*, 3061–3070. [CrossRef]
21. Sánchez, J.M.; López-Urrea, R.; Rubio, E.; González-Piqueras, J.; Caselles, V. Assessing Crop Coefficients of Sunflower and Canola Using Two-Source Energy Balance and Thermal Radiometry. *Agric. Water Manag.* **2014**, *137*, 23–29. [CrossRef]
22. Sánchez, J.M.; López-Urrea, R.; Doña, C.; Caselles, V.; González-Piqueras, J.; Niclòs, R. Modeling Evapotranspiration in a Spring Wheat from Thermal Radiometry: Crop Coefficients and E/T Partitioning. *Irrig. Sci.* **2015**, *33*, 399–410. [CrossRef]
23. Colaizzi, P.D.; Kustas, W.P.; Anderson, M.C.; Agam, N.; Tolk, J.A.; Evett, S.R.; Howell, T.A.; Gowda, P.H.; O'Shaughnessy, S.A. Two-Source Energy Balance Model Estimates of Evapotranspiration Using Component and Composite Surface Temperatures. *Adv. Water Resour.* **2012**, *50*, 134–151. [CrossRef]
24. González-Dugo, M.P.; González-Piqueras, J.; Campos, I.; Balbontín, C.; Calera, A. Estimation of Surface Energy Fluxes in Vineyard Using Field Measurements of Canopy and Soil Temperature. *Remote Sens. Hydrol.* **2010**, *352*, 59–62.
25. López-Urrea, R.; Sánchez, J.M.; Montoro, A.; Mañas, F.; Intrigliolo, D.S. Effect of Using Pruning Waste as an Organic Mulching on a Drip-Irrigated Vineyard Evapotranspiration under a Semi-Arid Climate. *Agric. For. Meteorol.* **2020**, *291*, 108064. [CrossRef]
26. Kustas, W.P.; Nieto, H.; Garcia-Tejera, O.; Bambach, N.; McElrone, A.J.; Gao, F.; Alfieri, J.G.; Hipps, L.E.; Prueger, J.H.; Torres-Rua, A.; et al. Impact of Advection on Two-Source Energy Balance (TSEB) Canopy Transpiration Parameterization for Vineyards in the California Central Valley. *Irrig. Sci.* **2022**, 1–17. [CrossRef]

27. Xia, T.; Kustas, W.P.; Anderson, M.C.; Alfieri, J.G.; Gao, F.; McKee, L.; Prueger, J.H.; Geli, H.M.E.; Neale, C.M.U.; Sanchez, L.; et al. Mapping Evapotranspiration with High-Resolution Aircraft Imagery over Vineyards Using One- and Two-Source Modeling Schemes. *Hydrol. Earth Syst. Sci.* **2016**, *20*, 1523–1545. [CrossRef]
28. Sánchez, J.M.; Simón, L.; González-Piqueras, J.; Montoya, F.; López-Urrea, R. Monitoring Crop Evapotranspiration and Transpiration/Evaporation Partitioning in a Drip-Irrigated Young Almond Orchard Applying a Two-Source Surface Energy Balance Model. *Water* **2021**, *13*, 2073. [CrossRef]
29. Lamm, F.R.; Colaizzi, P.D.; Sorensen, R.B.; Bordovsky, J.P.; Dougherty, M.; Balkcom, K.; Zaccaria, D.; Bali, K.M.; Rudnick, D.R.; Peters, R.T. A 2020 Vision of Subsurface Drip Irrigation in the U.S. *Trans. ASABE* **2021**, *64*, 1319–1343. [CrossRef]
30. Payero, J.O.; Yonts, C.D.; Irmak, S.; Tarkalson, D. EC05-776 Advantages and Disadvantages of Subsurface Drip Irrigation. In *Historical Materials from University of Nebraska-Lincoln Extension*; University of Nebraska-Lincoln: Lincoln, NE, USA, 2005; pp. 1–8.
31. Reich, D.; Godin, R.; Chávez, J.L.; Broner, I. *Subsurface Drip Irrigation (SDI)*; Colorado State University Extension; Colorado State University: Fort Collins, CO, USA, 2014; pp. 1–3.
32. Ayars, J.E.; Phene, C.J.; Phene, R.C.; Gao, S.; Wang, D.; Day, K.R.; Makus, D.J. Determining Pomegranate Water and Nitrogen Requirements with Drip Irrigation. *Agric. Water Manag.* **2017**, *187*, 11–23. [CrossRef]
33. Ma, X.; Sanguinet, K.A.; Jacoby, P.W. Direct Root-Zone Irrigation Outperforms Surface Drip Irrigation for Grape Yield and Crop Water Use Efficiency While Restricting Root Growth. *Agric. Water Manag.* **2020**, *231*, 105993. [CrossRef]
34. Romero, P.; Botia, P.; Garcia, F. Effects of Regulated Deficit Irrigation under Subsurface Drip Irrigation Conditions on Vegetative Development and Yield of Mature Almond Trees. *Plant Soil* **2004**, *260*, 169–181. [CrossRef]
35. USDA-NRCS. *Keys to Soil Taxonomy*, 12th ed.; United States Department of Agriculture: Washington, DC, USA, 2014.
36. USDA-ARS. Soil Water Characteristics Programme. Available online: https://www.ars.usda.gov/research/software/download/?softwareid=492&modecode=80-42-05-10%20 (accessed on 16 March 2022).
37. Trigo, I.F.; de Bruin, H.; Beyrich, F.; Bosveld, F.C.; Gavilán, P.; Groh, J.; López-Urrea, R. Validation of Reference Evapotranspiration from Meteosat Second Generation (MSG) Observations. *Agric. For. Meteorol.* **2018**, *259*, 271–285. [CrossRef]
38. SIAR Sistema de Información Climática Para el Regadío. Available online: https://eportal.mapa.gob.es/websiar/SeleccionParametrosMap.aspx?dst=1 (accessed on 16 March 2022).
39. Thomas, D. *Phenology Standard for Almonds*; Shouth Australian Resarch & Development Institute PIRSA: Adelaide, Australia, 2018.
40. Patrignani, A.; Ochsner, T.E. Canopeo: A Powerful New Tool for Measuring Fractional Green Canopy Cover. *Agron. J.* **2015**, *107*, 2312–2320. [CrossRef]
41. Auzmendi, I.; Mata, M.; Lopez, G.; Girona, J.; Marsal, J. Intercepted Radiation by Apple Canopy Can Be Used as a Basis for Irrigation Scheduling. *Agric. Water Manag.* **2011**, *98*, 886–892. [CrossRef]
42. Allen, R.G.; Pereira, L.S. Estimating Crop Coefficients from Fraction of Ground Cover and Height. *Irrig. Sci.* **2009**, *28*, 17–34. [CrossRef]
43. Villalobos, F.J.; De Melo-Abreu, J.P.; Mateos, L.; Fereres, E. The Radiation Balance. In *Principles of Agronomy for Sustainable Agriculture.*; Springer: Cham, Switzerland, 2016; pp. 27–41.
44. Fulton, A.; Grant, J.; Buchner, R.; Connell, J. *Using the Pressure Chamber for Irrigation Management in Walnut, Almond and Prune*; University of California, Agriculture and Natural Resources: Davis, CA, USA, 2014; ISBN 978-1-60107-858-2.
45. Fernández, J.E.; Alcon, F.; Diaz-Espejo, A.; Hernandez-Santana, V.; Cuevas, M.V. Water Use Indicators and Economic Analysis for On-Farm Irrigation Decision: A Case Study of a Super High Density Olive Tree Orchard. *Agric. Water Manag.* **2020**, *237*, 106074. [CrossRef]
46. Sainju, U.M.; Lenssen, A.W.; Allen, B.L.; Jabro, J.D.; Stevens, W.B. Crop Water and Nitrogen Productivity in Response to Long-Term Diversified Crop Rotations and Management Systems. *Agric. Water Manag.* **2021**, *257*, 107149. [CrossRef]
47. NCRS. Estimation of Direct Runoff from Storm Rainfall, Natural Resourcesconservation Service. In *Part 630 Hydrology. National Engineering Handbook*; United States Department of Agriculture: Washington, DC, USA, 2004.
48. Allen, R.G.; Pereira, L.S.; Smith, M.; Raes, D.; Wright, J.L. FAO-56 Dual Crop Coefficient Method for Estimating Evaporation from Soil and Application Extensions. *J. Irrig. Drain. Eng.* **2005**, *131*, 2–13. [CrossRef]
49. Fereres, E.; Goldhamer, D.A.; Sadras, V.O. Yield Response to Water of Fruit Trees and Vines: Guidelines. In *Crop Yield Response to Water*; FAO Irrigation and Drainage Paper; FAO: Rome, Italy, 2012; p. 505. ISBN 978-92-5-107274-5.
50. Sánchez, J.M.; Kustas, W.P.; Casselles, V.; Anderson, M.C. Modelling Surface Energy Fluxes over Maize Using a Two-Source Patch Model and Radiometric Soil and Canopy Temperature Observations. *Remote Sens. Environ.* **2008**, *112*, 1130–1143. [CrossRef]
51. R Core Team. R: A Language and Environment for Statistical Computing. Available online: https://www.R-project.org/ (accessed on 24 March 2021).
52. Espadafor, M.; Orgaz, F.; Testi, L.; Lorite, I.J.; Villalobos, F.J. Transpiration of Young Almond Trees in Relation to Intercepted Radiation. *Irrig. Sci.* **2015**, *33*, 265–275. [CrossRef]
53. Zhang, H.; Wang, D.; Ayars, J.E.; Phene, C.J. Biophysical Response of Young Pomegranate Trees to Surface and Sub-Surface Drip Irrigation and Deficit Irrigation. *Irrig. Sci.* **2017**, *35*, 425–435. [CrossRef]
54. Bryla, D.R.; Trout, T.J.; Ayars, J.E.; Johnson, R.S. Growth and Production of Young Peach Trees Irrigated by Furrow, Microjet, Surface Drip, or Subsurface Drip Systems. *HortScience* **2003**, *38*, 1112–1116. [CrossRef]

55. Lorite, I.J.; Cabezas-Luque, J.M.; Arquero, O.; Gabaldón-Leal, C.; Santos, C.; Rodríguez, A.; Ruiz-Ramos, M.; Lovera, M. The Role of Phenology in the Climate Change Impacts and Adaptation Strategies for Tree Crops: A Case Study on Almond Orchards in Southern Europe. *Agric. For. Meteorol.* **2020**, *294*, 108142. [CrossRef]
56. Espadafor, M.; Orgaz, F.; Testi, L.; Lorite, I.J.; González-Dugo, V.; Fereres, E. Responses of Transpiration and Transpiration Efficiency of Almond Trees to Moderate Water Deficits. *Sci. Hortic.* **2017**, *225*, 6–14. [CrossRef]
57. Egea, G.; Nortes, P.A.; González-Real, M.M.; Baille, A.; Domingo, R. Agronomic Response and Water Productivity of Almond Trees under Contrasted Deficit Irrigation Regimes. *Agric. Water Manag.* **2010**, *97*, 171–181. [CrossRef]
58. Girona, J.; Mata, M.; Marsal, J. Regulated Deficit Irrigation during the Kernel-Filling Period and Optimal Irrigation Rates in Almond. *Agric. Water. Manag.* **2005**, *75*, 152–167. [CrossRef]
59. Mañas, F.; López-Fuster, P.; López-Urrea, R. Effects of Different Regulated and sustained deficit irrigation strategies in almond production. *Acta Hortic.* **2014**, *1028*, 391–394. [CrossRef]
60. Gutiérrez-Gordillo, S.; Durán-Zuazo, V.H.; García-Tejero, I. Response of Three Almond Cultivars Subjected to Different Irrigation Regimes in Guadalquivir River Basin. *Agric. Water Manag.* **2019**, *222*, 72–81. [CrossRef]
61. Goldhamer, D.A.; Fereres, E. Establishing an Almond Water Production Function for California Using Long-Term Yield Response to Variable Irrigation. *Irrig. Sci.* **2017**, *35*, 169–179. [CrossRef]